Electronic structure of WSe_2: A combined photoemission and inverse photoemission study

M. Traving, M. Boehme, L. Kipp,* and M. Skibowski
Institut für Experimentalphysik, Universität Kiel, D-24098 Kiel, Germany

F. Starrost, E. E. Krasovskii,† A. Perlov,† and W. Schattke
Institut für Theoretische Physik, Universität Kiel, D-24098 Kiel, Germany

(Received 2 August 1996)

We report on a complete determination of the experimental and theoretical valence- and conduction-band structure of WSe_2. The results of combined angle-resolved photoemission and inverse photoemission are discussed in the context of fully relativistic linear-muffin-tin-orbital and extended linear-augmented-plane-wave calculations. We measure an indirect band gap of 1.2 eV, and find the valence-band maximum to be located at the center of the Brillouin zone and the conduction-band minimum at 0.55ΓK.
[S0163-1829(97)02216-9]

I. INTRODUCTION

The atomic and electronic structures of transition-metal dichalcogenides have been the subject of many experimental and theoretical investigations.[1–5] Tungsten diselenide, with a fundamental band gap of 1.2 eV, being one of the semiconducting layered compounds, may be viewed as prototype material for optoelectronic and photovoltaic devices. In fact, solar cells with efficiencies up to 17% have been reported.[6]

A comprehensive understanding of the electronic properties of those materials is crucial for further progress in this field. Band-structure calculations within the local-density approximation (LDA) (Ref. 7) predict an indirect fundamental gap, as also observed in optical experiments.[8] The position of the valence-band maximum, however, has been controversially discussed recently.[9] The LDA calculation of Coehoorn *et al.*[7] predicts the valence-band maximum (VBM) to be located at the center of the Brillouin zone. Recent photoemission results, in contrast, seem to give evidence of a VBM located at K on the zone boundary in line with a full-potential LDA band-structure calculation.[9]

It is the aim of the work presented in this paper to make a detailed study of the occupied and unoccupied electronic structure of WSe_2. The experimental band structure and band gap resulting from combined angle-resolved photoemission and inverse photoemission spectroscopy will be analyzed in comparison to band-structure calculations using the relativistic linear muffin tin orbital (RLMTO) and the extended linear-augmented-plane-wave (ELAPW) methods.

The second section deals with the structural and electronic properties of WSe_2. After describing the experimental details, we will discuss the experimental determination of the valence-band maximum and conduction band minimum (CBM). This is followed by a description and the results of the band-structure calculations. A comprehensive discussion of the occupied and unoccupied experimental band structure will be presented and compared with theory in Sec. VI.

II. STRUCTURAL AND ELECTRONIC PROPERTIES

The macroscopic and microscopic properties of the layered crystal WSe_2 show a pronounced two-dimensional character. While inside one layer the strong ionic and covalent bonding predominates, weak van der Waals forces act between the layers. Consequently, the transition-metal dichalcogenides exhibit strong anisotropic properties (e.g., in optical and electronic properties).

Inside one layer the transition-metal atom W is hexagonally surrounded by six other W atoms. This plane of metal atoms is sandwiched by two layer planes of hexagonal close packed Se atoms. The chalcogen atoms are coordinated trigonal prismatic with regard to the transition metal atom, as shown in Fig. 1(a). Different stacking sequences of the layers result in the polymorphic types of the crystals with different lattice parameters c perpendicular to the layers. WSe_2 crystallizes in the $2H$ structure, i.e., two sandwiches contribute to c. The lattice parameters for WSe_2 are $a=3.286$ Å and $c=2\times 6.488$ Å.[5] WSe_2 belongs to the nonsymmorphic space group $P6_3/mmc$. Figure 1(b) shows the corresponding Brillouin zone of WSe_2. Capitals denote points of high symmetry.

According to Liang,[1] the electronic structure of WSe_2 can be pictured as follows. The energetically lowest states with mainly Se $4s$ and Se $4p$ character are fully occupied. Because W belongs to the transition-metal group VIb, the intralayer bondings show mainly covalent character. In this case the trigonal prismatic coordination is favored. For energetical reasons the fully occupied W $5d_{z^2}$ band splits off from the remaining unoccupied W $5d$ bands, and shifts to lower energies. It causes a band gap of about 1.2 eV, fol-

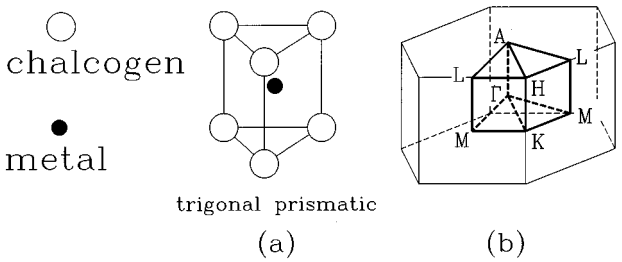

FIG. 1. (a) Trigonal prismatic coordination of the Se atoms in $2H$-WSe_2. (b) Brillouin zone of WSe_2.

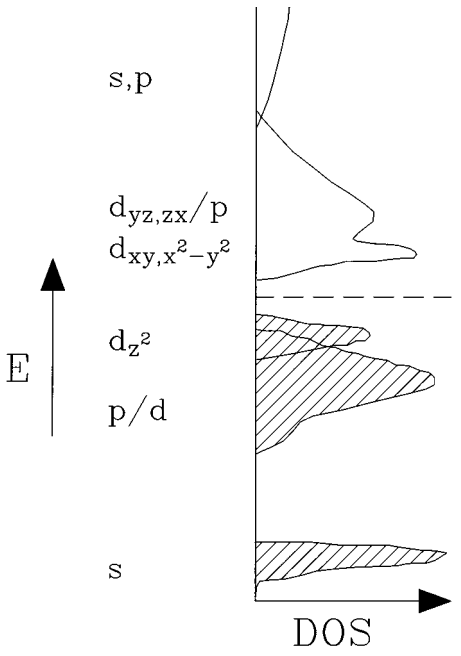

FIG. 2. Schematic density of states of WSe_2 in the trigonal prismatic $2H$ phase [after Liang *et al.* (Ref. 1)].

lowed by the unoccupied s and p states with the main contribution from the cation (see Fig. 2).

III. EXPERIMENT

The angle-resolved photoemission spectra were taken at the HONORMI beamline of the DORIS III storage ring at Hamburg Synchrotron Radiation Laboratory for photon energies 9 eV$<h\nu<$33 eV. The electrons were detected by use of a 180° spherical analyzer mounted on a goniometer which is movable around two independent axes. These degrees of freedom allow a very accurate final sample adjustment performed by taking spectra in small-angle steps around the critical points without moving the sample. For the spectra shown here, an overall energy resolution of 50 meV$<\Delta E<$130 meV and an angle resolution $\Delta\vartheta<0.25°$ were chosen.

The inverse photoemission spectra were taken by using a compact grating spectrometer with parallel detection of photons in the energy range of 10 eV$\leqslant h\nu\leqslant$40 eV.[10,11] Electrons were focused on the sample by an Erdman-Zipf-type electron gun[12] with $\sim$ 1-mm^2 spot size and angle divergence $<3°$. Energy and momentum resolutions are typically 400 meV and 0.05 Å^{-1}.

In order to refer energies to the experimentally determined VBM, we apply combined angle resolved photoemission and inverse photoemission (CARPIP) spectroscopy.[11] In this technique a common energy scale for angle-resolved photoemission and inverse photoemission data is established by detecting the electron energy from the inverse photoemission electron gun with the photoemission electron energy analyzer. Thus a separate determination of the Fermi level as reference energy is avoided, and band bending does not affect the calibration. This technique therefore allows a very accurate determination of energy differences between occupied and unoccupied states including the fundamental band gap.

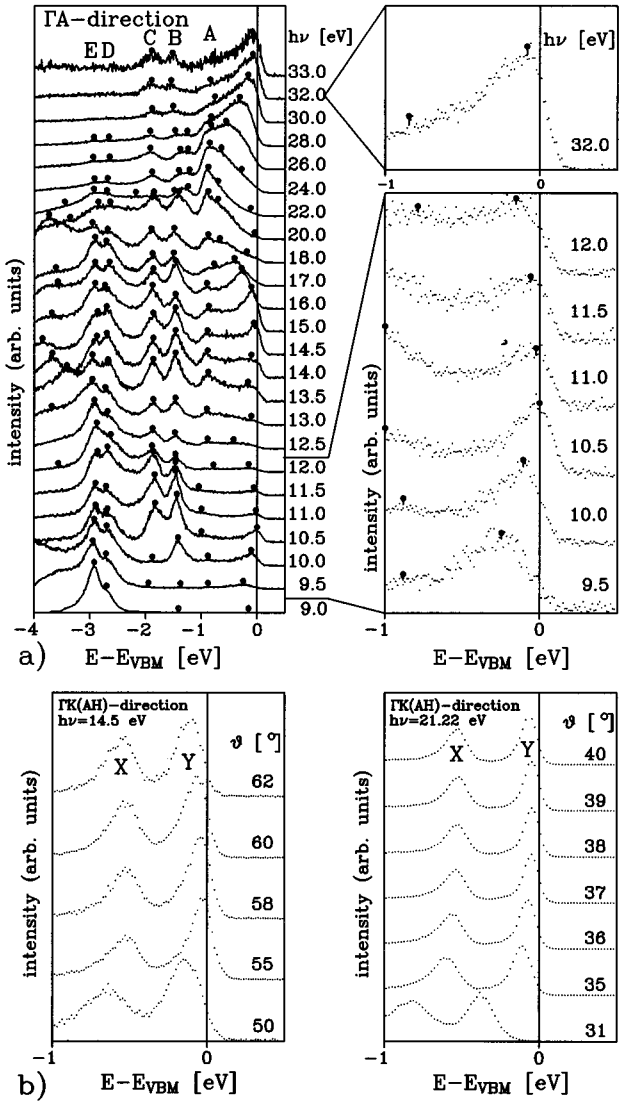

FIG. 3. (a) Normal-emission photoelectron spectra of WSe_2 taken in the EDC mode. The capitals mark dispersionless emissions. The enlarged panels display the energetically highest emissions showing a maximum at 10.5 eV. (b) EDC spectra around the $K(H)$ point in the $\Gamma K(AH)$ direction near the Fermi energies at $h\nu=14.5$ and 21.22 eV.

$2H$-WSe_2 crystals were grown by chemical vapor transport using iodine as transport gas. According to Hall measurements the crystals were strongly p doped ($p=2\times10^{17}$ cm^{-3} at $T=300$ K). Clean WSe_2 surfaces were prepared by cleavage parallel to the weakly bonded sandwich layers. The crystal quality was characterized by Laue x-ray diffraction, low-energy electron diffraction, scanning tunneling microscopy, and the surface sensitivity of photoemission and inverse photoemission itself.

IV. DETERMINATION OF VBM AND CBM

For a discussion of electronic properties in the context of band-structure calculations it is essential to have an accurate experimental knowledge of the VBM, which serves as energy reference for a direct comparison of experimental and

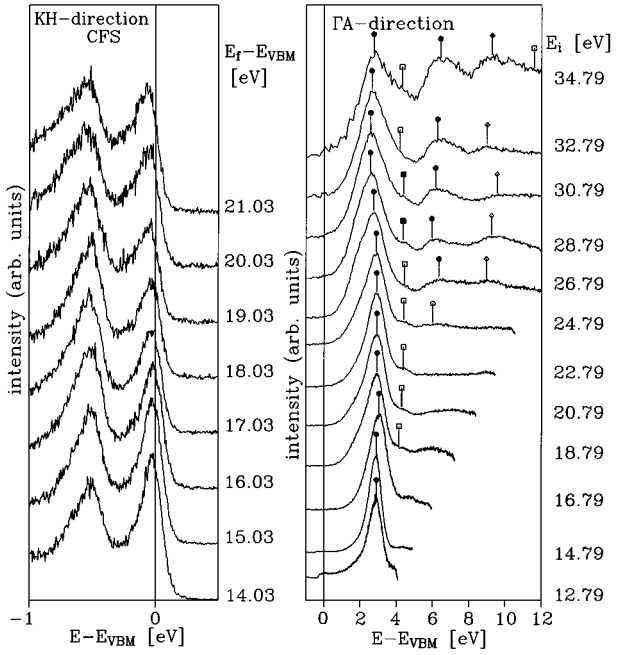

FIG. 4. (a) CFS spectra of WSe_2 in the KH direction ($k_\parallel = |\Gamma K|$), (b) ARICIS spectra in the ΓA direction ($k_\parallel = 0.0$).

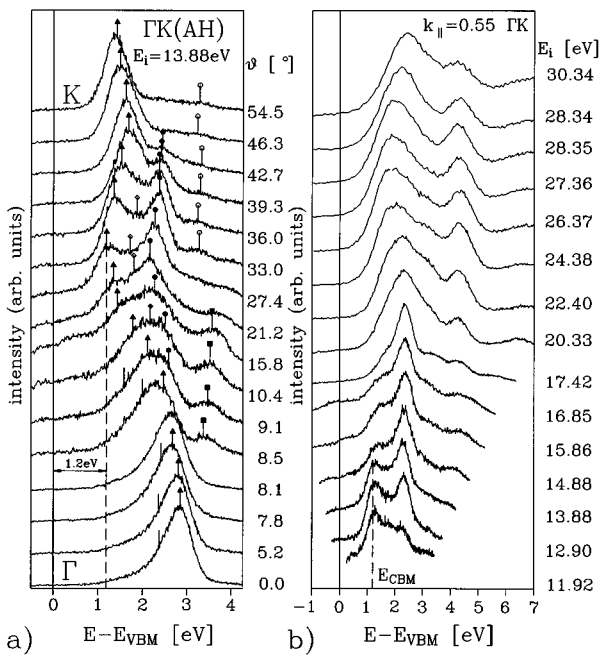

FIG. 5. (a) ARICIS spectra taken at initial energy $E_i = 13.88$ eV in the $\Gamma K(AH)$ direction. The dashed line indicates the band gap. Energies refer to the VBM. (b) ARICIS spectra of WSe_2 taken at $k_\parallel = 0.55\Gamma K$. The dashed line marks the energy of the lowest unoccupied band.

theoretical results. An appropriate tool for an experimental determination are measurements of energy distribution curves (EDC's) for various photon energies by means of angle-resolved photoemission spectroscopy (see, e.g., Refs. 13–15).

In Fig. 3(a) we show normal-emission ($\vartheta = 0°$) photoelectron spectra taken in the EDC mode using synchrotron radiation. Upon changing the photon energy, the $k_\perp$ component is varied along the ΓA direction of the Brillouin zone.

According to theory, the electronic structure of layered materials should show no or only weak dispersion perpendicular to the layers. This strong two-dimensional character can be clearly observed in the photoemission spectra of Fig. 3(a). The binding energies of the emissions labeled A, B, C, D, and E remain almost at constant binding energy when the photon energy is changed.

In angle-resolved photoemission spectra the valence-band maximum is determined by the energetically highest emission feature. The high-resolution spectra shown in the enlarged panels of Fig. 3(a) locate the VBM at 10.5-eV photon energy.

High-resolution spectra taken around the $K(H)$ point of the Brillouin zone for photon energies of 14.5 and 21.22 eV are plotted in Fig. 3(b). We observe two emission features X and Y showing distinct dispersion around $K(H)$. The highest energy of Y, however, is well below the highest occupied energy level at Γ, i.e., it is determined to be 30 meV below the VBM. In order to investigate $k_\perp$ effects, we measured along the $K(H)$ direction of the Brillouin zone [Fig. 4(a)]. The spectra are taken in the constant-final-state (CFS) mode, i.e., the final-state energy of the detected electrons is kept constant, while the photon energy is swept. In contrast to an EDC spectrum, in a CFS spectrum the $k_\parallel$ component is constant. The double structure exhibits very weak dispersion in the KH direction (in agreement with theory). The upper emission Y at $K(H)$ remains energetically below the peak at $\Gamma(A)$ at $h\nu = 10.5$ eV by $\Delta E = 30$ meV. This clearly demonstrates that experimentally that the VBM is observed at the center of the Brillouin zone, i.e., at the Γ point. In contrast, Straub *et al.*[9] recently observed the highest emission at K. Their conclusion was derived from a limited data set containing only spectra at photon energies above 21 eV which compare well with our results. However, we observe the VBM for a spectrum taken at 10.5-eV photon energy.

Applying CARPIP allows us to establish a common unique energy scale for photoemission and inverse photoemission spectra. Thus band gaps can be determined with high accuracy without referring to the Fermi energy explicitly. In order to investigate the conduction band minimum we first took spectra in the angle-resolved inverse constant initial energy spectroscopy (ARICIS) mode in directions ΓA (perpendicular to the layers) and ΓK (parallel to the layers). A selection of these spectra is shown in Figs. 4(b) and 5(a). In direction ΓA [see Fig. 4(b)], we observe a pronounced peak about 2.8 eV above the VBM, showing only weak dispersion. By tracing this peak along ΓK [see Fig. 5(a)], we observe a splitting around $\frac{1}{4}\Gamma K$, and find the lowest conduction band dispersing down in energy to 1.2 eV above the VBM. We found the CBM at $k_\parallel = 0.55\Gamma K$ and $E_i = 13.88$ eV after variation of $k_\parallel$ and $k_\perp(E_i)$ around these values (see Fig. 5). The resulting fundamental band gap of WSe_2 is indirect and has a value of 1.2 eV, in line with optical data.[8]

V. BULK BAND-STRUCTURE CALCULATION

We calculated the band structure of WSe_2 self-consistently within the local-density approximation, employ-

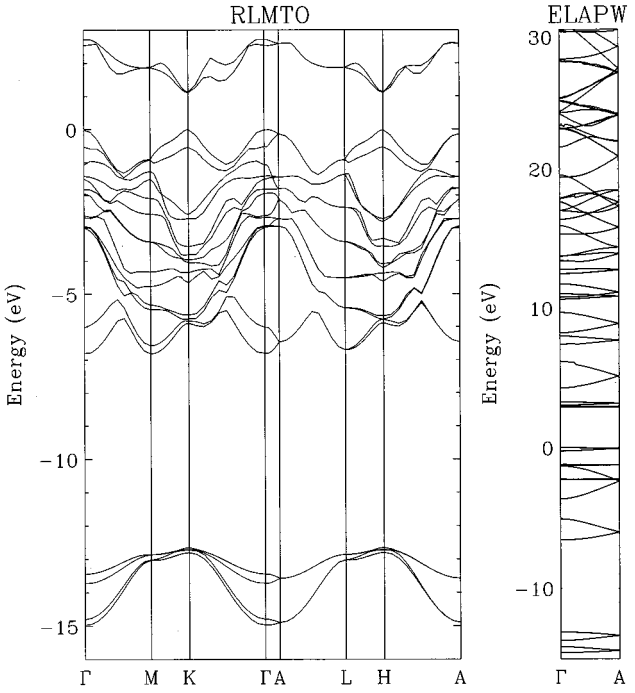

FIG. 6. Band structure of WSe_2 calculated by the fully relativistic RLMTO method (on the left). Energy bands along the ΓA direction according to the scalar-relativistic ELAPW method (on the right). In both graphs the valence-band maximum is chosen as the energy zero.

ing two techniques. For the valence bands we used the fully relativistic LMTO,[16,17] and for the conduction bands we applied the scalar-relativistic extended LAPW,[18] which, because of the use of an extended basis set, is more accurate for higher energies.[19] For both methods we use a basis of six atoms and two empty spheres as in Ref. 7, with $z=0.125$, where z is the fractional distance between metal and nonmetal layers in units of c.

The RLMTO calculations were carried out with basis functions including angular momenta up to $l=3$ for W, $l=2$ for Se, and $l=1$ for the empty spheres. The non-*ASA* contribution to the overlap matrix, i.e., the so-called combined correction, was taken into account.[20] In the ELAPW the set of basis functions was made up of all APW's with reciprocal-lattice vectors $\vec{G}$ for which $|\vec{G}|S<7.41$, S being the muffin-tin spheres' radius which in this case was $S=2.358$ a.u. for all the spheres. This yielded 439 usual APW's, and as a result of the extension there were 50 additional functions.

As WSe_2 has an inert (0001) surface, only bulk band-structure calculations have been carried through. Both energy regimes, the valence as well as an extended conduction-band range, are considered, because with the knowledge of the final photoemission states electron-transition (ET) plots can be constructed. These plots assist the interpretation within the band mapping framework, and are indispensable for reliable statements on the band structure, as long as calculations within the photoemission one-step model are not available.

The electron transition plots (see Figs. 7 and 8) are derived from the LMTO valence bands (Fig. 6, left) and ELAPW conduction bands, which we show only in the ΓA direction (Fig. 6, right). The ELAPW valence-band part is only presented for comparison and completeness. Free-electron-like branches folded back at the zone boundaries appear for high energies, besides a series of gaps and less dispersive bands below 15 eV. In the APW decomposition the free-electron-like bands are frequently associated with wave vectors perpendicular to the layer planes only. However, different from the well-known normal-emission finding that forward emission often dominates the photocurrent, here we could not detect such a behavior. In contrast, the electron transition plots to be discussed in the following show that the electron emissions accumulate rather from the regions of high one-dimensional density of states, as given by the band edges or by the low dispersive bands.

In the RLMTO calculations we find the valence-band maximum at K, while the highest valence band at Γ is only 18 meV below. The CBM is also at K, so that we obtain a direct band gap of 1.1 eV. The ELAPW method places the VBM at Γ. It is significantly higher in energy than the highest valence band at K. This calculation yields a CBM at 0.55 ΓK, and an indirect band gap of about 0.4 eV. Considering the position of the VBM, the RLMTO results do not discriminate between the Γ and K points (a 18-meV difference), whereas the ELAPW puts the VBM at Γ (a 224-meV difference). Because of the lack of fully relativistic treatment in the latter, we cannot finally decide on the position from a theoretical point of view.

VI. RESULTS AND DISCUSSION

A. Electronic structure along ΓA

In order to investigate the occupied and unoccupied electronic structures perpendicular to the layers, we employed angle-resolved photoemission and inverse photoemission at $k_{\parallel}=0$, while varying the stimulating photon energy (photoemission) and initial electron energies (inverse photoemission). In photoemission and inverse photoemission, respectively, the value of $k_{\perp}$ is thereby unknown because of the broken translational symmetry perpendicular to the surface. However, suitable assumptions on the part of the band structure complementary to that under investigation (e.g., free-electron-like final states in the case of photoemission) allow, in principle, a determination of the perpendicular component of the wave vector $k_{\perp}$ within the direct transition model. Furthermore, it is not even necessary to determine $k_{\perp}$ because one can display initial-state energies of spectral features as a function of the corresponding final-state energies. The obtained ET plots[14] allow the experimental results to be directly compared with theory, if, of course, a theoretical band structure has already been calculated. Such a comparison between experimental data and the theoretical transitions in the ΓA direction is shown in Fig. 7.

On the part of the theory, all possible transitions between occupied initial states and unoccupied final states have been plotted (regardless of selection rules). The experimental data were drawn with $E_B=0$ eV equal to the VBM of theory. One clearly detects horizontal empty stripes corresponding to gaps between valence bands and, for low final-state energies, also empty vertical stripes derived from gaps between conduction bands. Many experimental emissions arise near the

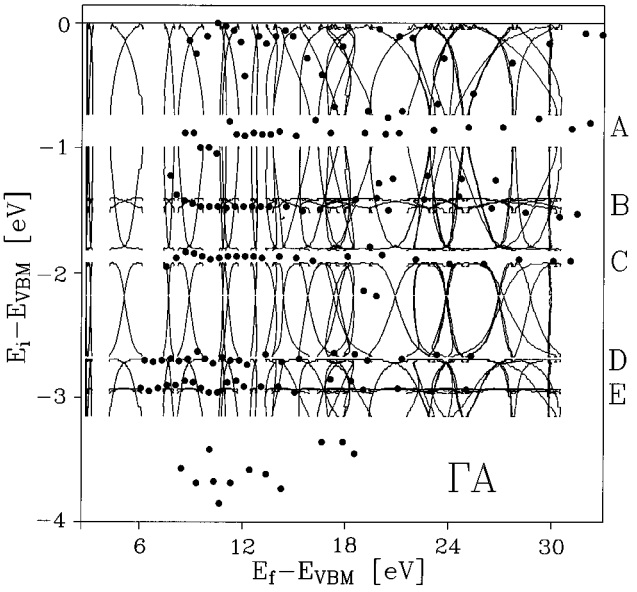

FIG. 7. Electron transition plot of the valence bands in the ΓA direction of WSe_2. Filled circles represent the experimental data, solid lines the theoretically possible photoemission transitions using the RLMTO calculation for the valence bands and the ELAPW calculation for the conduction bands.

band edges and from less dispersive bands, such as around 0, -1.5 [feature B of Fig. 3(a)], $-1.8(C)$, $-2.7(D)$, and -3 eV(E). Additional data points are found in the gap near -1 eV (feature A), which could also be attributed to the neighboring band edges, and within the large gap between -3.2 and -6 eV (see Fig. 6, left). The latter could be connected with valence states if the ELAPW calculation had

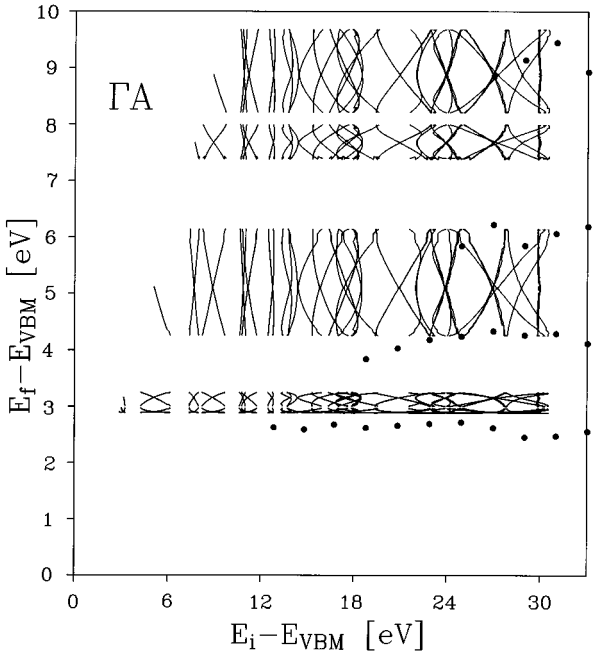

FIG. 8. Electron transition plot for inverse photoemission showing transitions from unoccupied states in the ΓA direction of WSe_2. Solid lines represent theoretically possible transitions. Experimental data are plotted by filled circles.

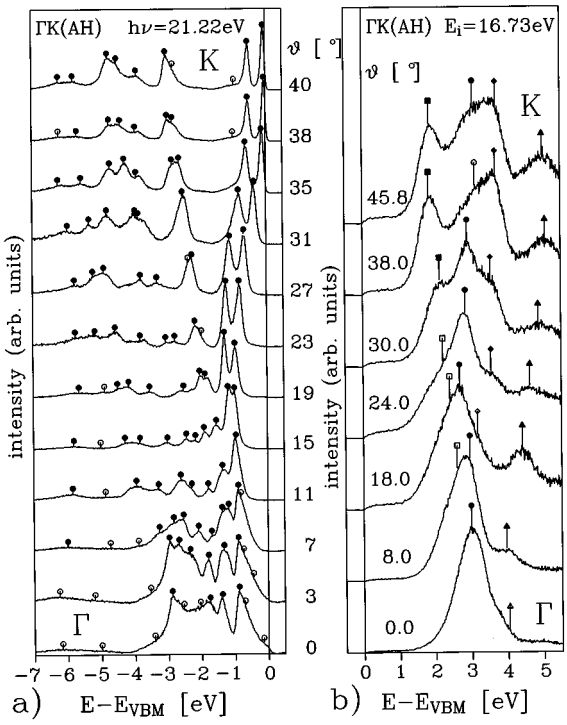

FIG. 9. (a) EDC spectra in the $\Gamma K(AH)$ direction for a photon energy $h\nu = 21.22$ eV. (b) ARICIS spectra in the $\Gamma K(AH)$ direction taken at an initial electron energy $E_i = 16.73$ eV.

also been used for the valence bands. Former LAPW results[9] would also yield some states within this gap. At present, the calculations are too much at variance on this highly expanded energy scale to decide which deficiency of the method may be responsible for the failure between -3 and -4 eV. Apart from this question the general agreement between experiment and theory seen in Fig. 7 appears to be very good. In particular, the accurate positions (see structures B, C, D, and E in Fig. 7) of the additional spin-orbit-split nondispersive bands show that the RLMTO gives a reliable explanation of the experimental results.

The ARICIS spectra in the ΓA direction [Fig. 4(b)] show dispersionless emission features as observed in the occupied band structure [Fig. 3(a)]. The corresponding comparison with theory is shown in the ET plot in Fig. 8. As in Fig. 7, all possible transitions between initial and final bands have been plotted regardless of selection rules. The strong peak at $E_B = 2.8$ eV marked by filled circles in Fig. 4(b) is found at slightly lower binding energies than theory predicts. The next two, energetically higher emissions [in Fig. 4(b), marked by squares and circles] coincide with the band edges of the final bands of the ELAPW calculation at $E_B = 4.2$ and 6.2 eV, respectively. Therefore, one concludes that the theory can account for the dispersionless states observed in the ΓA direction.

B. Electronic structure along $\Gamma K(AH)$

In order to determine the band structure in the $\Gamma K(AH)$ and $\Gamma M(AL)$ directions, we measured off-normal emission (EDC) as well as off-normal incidence (ARICIS) spectra.

Figure 9(a) shows EDC spectra in the $\Gamma K(AH)$ direction taken at $h\nu = 21.22$ eV. With increasing polar angle ϑ, the

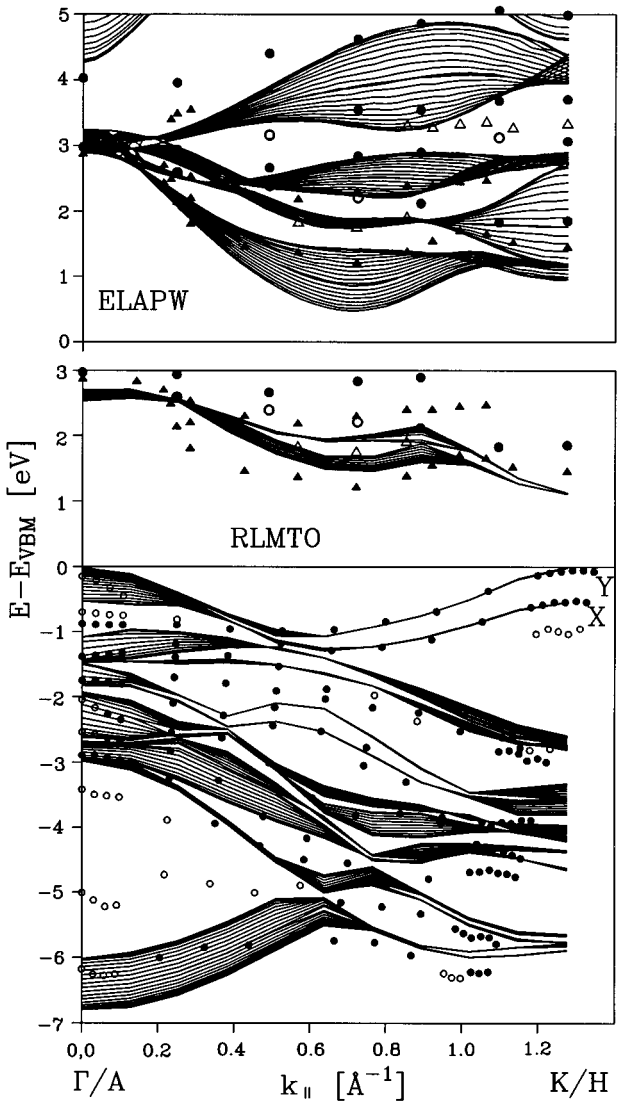

FIG. 10. Comparison of the occupied (circles) and unoccupied band structure ($E_i = 13.88$-eV triangles, $E_i = 16.73$-eV circles) in the $\Gamma K(AH)$ direction with a projection of the RLMTO theory (occupied and lower unoccupied states) and the ELAPW method (unoccupied states). Filled symbols indicate strong emissions, empty symbols weak emissions.

previously mentioned characteristic peaks X and Y arise. They disperse to smaller binding energies, when $k_{\parallel}$ approaches the $K(H)$ point.

Figure 9(b) presents a selection of ARICIS spectra in the $\Gamma K(AH)$ direction taken at the initial electron energy $E_i = 16.73$ eV. Four different bands can be traced in the $\Gamma K(AH)$ direction, marked by different symbols. In contrast to Fig. 5(a), the spectra in Fig. 9(b) exhibit no clear minimum in the $\Gamma K(AH)$ direction at this different electron energy.

The comparison of the occupied and unoccupied band structures in the $\Gamma K(AH)$ direction with theory is shown in Fig. 10. The experimental valence-band structure at a photon energy of $h\nu = 21.22$ eV is plotted onto the projected valence band structure of the RLMTO method.[20]

On the part of the conduction-band structure, we plotted the experimental results for the initial electron energies

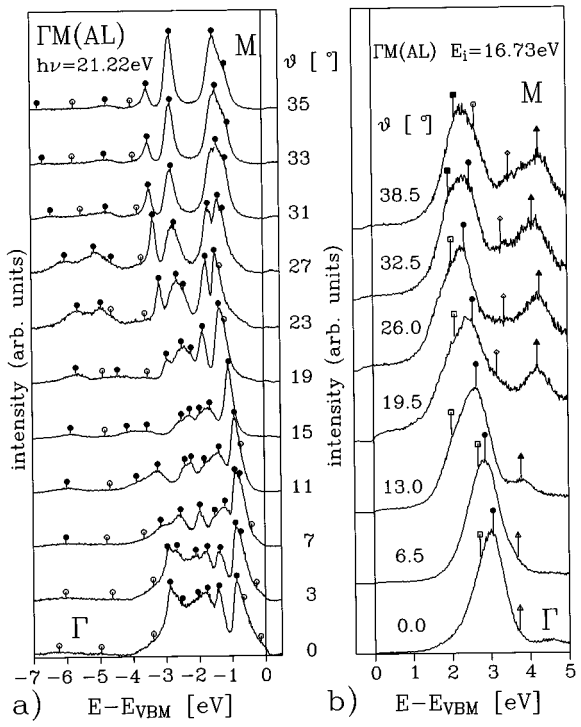

FIG. 11. (a) EDC spectra in the $\Gamma M(AH)$ direction excited with a photon energy of $h\nu = 21.22$ eV. (b) ARICIS spectra in the $\Gamma M(AL)$ direction taken at an initial electron energy $E_i = 16.73$ eV.

$E_i = 13.88$ eV (triangles) and $E_i = 16.73$ eV (circles) onto the projected band structures of the RLMTO method (upper part of lower panel, Fig. 10) and the ELAPW method (upper panel).

A satisfactory agreement with the experimental data points, especially with respect to the strong peaks, is observed in direction ΓK. The double structure X, Y shows an excellent agreement with the theoretical bands from $0.5\Gamma K$ to the $K(H)$ point. Even the splitting of the structure is described correctly, indicating the importance of the fully relativistic calculation. The very narrow bands of the double structure in theory confirm the lack of $k_{\perp}$ dispersion of the double structure, as seen in Fig. 4(a). At K, in the RLMTO calculations, the uppermost valence-band state is found to be slightly higher by 18 meV than at Γ, whereas in the experiment we found the VBM at Γ with an energy difference of 30 meV to K (see Sec. IV). (In the ELAPW method, the comparison with experimental valence-band data suffers from neglecting spin-orbit coupling. However, that calculation yields the VBM at Γ, with 224 meV above the maximum at K.)

The lowest unoccupied band as calculated by the RLMTO coincides well with the corresponding data points (lower panel). In the upper panel the results of the scalar-relativistic generalized LAPW method for the lower conduction bands are plotted. The generalization guarantees a higher accuracy regarding the agreement with the original nonlinear APW.[19] This applies especially to the higher-energy bands up to 30 eV, where the method is superior to the RLMTO calculation. Those bands are necessary for drawing the ET plots. However, the method yields a CBM which seems to be too low. The experimentally found CBM between Γ and K better agrees with the ELAPW results if the bands are rigidly

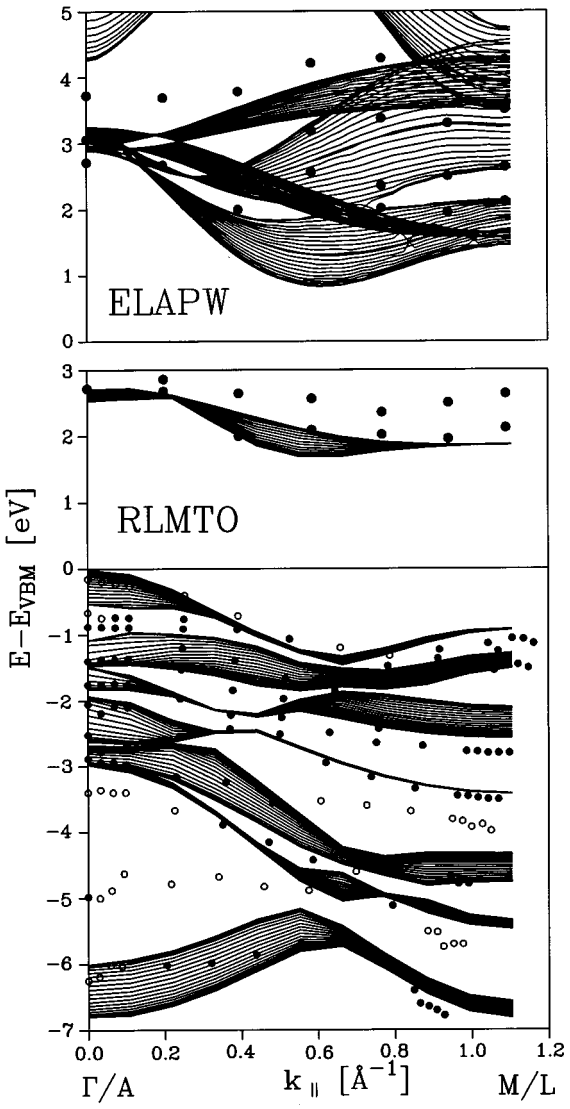

FIG. 12. Comparison of the occupied and unoccupied band structures ($E_i = 16.73$ eV) in the $\Gamma M(AL)$ direction with a projection of the RLMTO theory (occupied and lower unoccupied states) and the ELAPW method (unoccupied states). Filled symbols indicate strong emissions, empty symbols weak emissions.

shifted by roughly 0.5 eV to higher energies, which may be attributed to quasiparticle effects opening the main gap. But the same effects could also affect the position of the VBM and CBM by changing the dispersion; see, e.g., Wenzien, Cappellini, and Bechstedt.[21] Thus the solution of these questions depending on such tiny energy differences is postponed to further computations.

In spite of the fact that, as previously mentioned, the calculated band gap is too small (LDA), the lowest experimental conduction band shows the same dispersion as the lowest band of the ELAPW calculation in the ΓK direction. At approximately $0.55\Gamma K$ it runs through a minimum, before it disperses to higher energy. Approaching the $K(H)$ point, it shifts clearly to lower energy again, in agreement with our theory.

C. Electronic structure along $\Gamma M(AL)$

The evolution of the emissions in the $\Gamma M(AL)$ direction at $h\nu = 21.22$ eV is shown in Fig. 11(a). A selection of ARICIS spectra in the $\Gamma M(AL)$ direction for the initial energy $E_i = 16.73$ eV is presented in Fig. 11(b).

The corresponding comparison with the projected band structures of the RLMTO calculation and the ELAPW method is shown in Fig. 12. Again we note a good agreement between theory and experiment as in the $\Gamma K(AH)$ direction. This is particularly true for the strong emissions, which are indicated by filled circles. Considering the conduction states, a slight shift of the theoretical bands to higher energies due to quasiparticle effects would improve the comparison here also.

VII. CONCLUSIONS

In summary we have employed CARPIP together with RLMTO and ELAPW calculations to determine the valence- and conduction-band structure of the layered material WSe_2. The experimental results yield an indirect fundamental band gap of 1.2 eV. The VBM is observed at the zone center Γ, while the CBM is found at $0.55\Gamma K$. The comparison of experiment and theory along ΓA by means of electron transition plots demonstrates an excellent agreement. Emissions mainly arise near band edges and from less dispersive bands, confirming the theoretically predicted effects of spin-orbit coupling. For $k_\parallel$ dispersions along ΓM and ΓK, we observe satisfactory agreement. In particular the splitting of the upper valence bands around K is correctly described by theory, demonstrating the importance of the fully relativistic calculation.

ACKNOWLEDGMENTS

We acknowledge experimental support by D. Kampfenger, J. Brügmann, and N. Trares-Wrobel. We would also like to thank R. Schwedhelm concerning computational questions, and A. Klein (HMI/Berlin) for the Hall measurements. This work was supported by the Bundesministerium für Bildung, Wissenschaft, Forschung und Technologie (Project Nos. 05 622 FKB, 05 605 FKB, and 05 605 FKA).

*Author to whom correspondence should be addressed.
†Permanent address: Institute of Metal Physics, Ukrainian Academy of Sciences, Vernadskogo 36, 252180 Kiev–142, Ukraine.

[1] W. Y. Liang, *Electronic Properties of Transition Metal Dichalcogenides and their Intercalation Complexes*, Vol. 148 of *NATO Advanced Study Institute, Series B: Intercalation in Layered Materials*, edited by M. S. Dresselhaus (Plenum, New York, 1986).
[2] J. A. Wilson and A. D. Yoffe, *The Transition Metal Dichalcogenides. Discussion and Interpretation of the Observed Optical, Electrical and Structural Properties*, Advances in Physics Vol. 18 (Taylor & Francis, London, 1969).
[3] R. Friendt and A. Yoffe, *Electronic Properties of Intercalation Complexes of the Transition Metal Dichalcogenides*, Advances in Physics Vol. 36 (Taylor & Francis, London, 1987).
[4] J. Phys. C **20**, 4019–4447 (1987).

[5] R. Manzke and M. Skibowski, in *Electronic Structure of Solids: Photoemission Spectra and Related Data*, edited by A. Goldmann, Landolt-Börnstein, New Series, Group III, Vol. 23, Pt. b (Springer Verlag, Berlin, 1994), p. 84.
[6] G. Prasad and O. Srivastava, J. Phys. D **21**, 1028 (1988).
[7] R. Coehoorn, C. Haas, J. Dijkstra, C. J. Flipse, R. A. de Groot, and A. Wold, Phys. Rev. B **35**, 6195 (1987).
[8] K.-K. Kam, C.-L. Chang, and D. W. Lynch, J. Phys. C **17**, 4031 (1984).
[9] Th. Straub, K. Fauth, Th. Finteis, M. Hengsberger, R. Claessen, P. Steiner, S. Hüfner, and P. Blaha, Phys. Rev. B **53**, R16 152 (1996).
[10] L. Kipp, M. Boehme, H. Carstensen, R. Claessen, and M. Skibowski, Rev. Sci. Instrum. (to be published).
[11] M. Skibowski and L. Kipp, J. Electron Spectrosc. Relat. Phenom. **68**, 77 (1994).
[12] P. W. Erdman and E. C. Zipf, Rev. Sci. Instrum. **53**, 225 (1982).
[13] R. Manzke, H. Barnscheidt, C. Janowitz, and M. Skibowski, Phys. Rev. Lett. **58**, 610 (1987).
[14] L. Kipp, R. Manzke, and M. Skibowski, Proc. SPIE **1361**, 794 (1991).
[15] L. Kipp, R. Manzke, and M. Skibowski, Solid State Commun. **93**, 603 (1995).
[16] O. K. Andersen, Phys. Rev. B **12**, 3060 (1975).
[17] V. V. Nemoshkalenko, A. A. Krasovsky, V. N. Antonov, Vl. N. Antonov, U. Fleck, H. Wonn, and P. Ziesche, Phys. Status Solidi B **120**, 283 (1982).
[18] E. E. Krasovskii and W. Schattke, Solid State Commun. **93**, 775 (1995).
[19] E. E. Krasovskii, A. N. Yaresko, and V. N. Antonov, J. Electron Spectrosc. Relat. Phenom. **68**, 157 (1994).
[20] V. N. Antonov, A. I. Bagljuk, A. Ya. Perlov, V. V. Nemoshkalenko, Vl. N. Antonov, O. K. Andersen, and O. Jepsen, Low Temp. Phys. **19**, 494 (1993).
[21] B. Wenzien, G. Cappellini, and F. Bechstedt, Phys. Rev. B **51**, 14 701 (1995).